



First Type III Solar Radio Bursts of Solar Cycle 25

Juha Kallunki¹ · Derek McKay^{1,2,3} ·
Merja Tornikoski¹

Received: 15 January 2021 / Accepted: 16 February 2021 / Published online: 6 April 2021
© The Author(s) 2021

Abstract The minimum of the previous solar cycle, Solar Cycle 24, occurred in December 2019, which also marked the start of the new Solar Cycle 25. The first radio bursts of the new solar cycle were observed in the spring season 2020. In this work we will present three type III solar bursts which were observed in May and June 2020 at radio frequencies between 18–90 MHz. There are two radio observatories in Finland that are capable of doing low-frequency solar radio observations: Aalto University Metsähovi Radio Observatory (MRO) and Kilpisjärvi Atmospheric Imaging Receiver Array (KAIRA) of the Sodankylä Geophysical Observatory, University of Oulu. The instruments of the two institutes have different design and characteristics, and they operate in rather different radio interference environments. We will compare simultaneous observations from these two instruments and we will also discuss the properties of these type III solar bursts.

Keywords Corona, radio emission · Instrumentation and data management · Radio bursts, type III

1. Introduction

Type III solar radio bursts can be detected at low radio frequencies even if the Sun is ostensibly quiet. Thus they are the most frequently observed solar radio emission feature. It has been noticed that the origin of type III bursts can sometimes be located near coronal

✉ J. Kallunki
juha.kallunki@aalto.fi

D. McKay
derek.mckay@utu.fi

M. Tornikoski
merja.tornikoski@aalto.fi

¹ Aalto University Metsähovi Radio Observatory, Metsähovintie 114, 02540 Kylmälä, Finland

² Turku University, FINCA, Vesilinnantie 5, 20014 Turun yliopisto, Finland

³ Sodankylä Geophysical Observatory, University of Oulu, Tähteläntie 62, 99600 Sodankylä, Finland

holes (Alissandrakis et al., 2015). However, they usually come from solar active regions. Type III bursts are a signature of beams of energetic electrons traveling through the corona. They have a fast drifting radio emission structure, even up to 100 MHz/s. Type III bursts have been observed at a wide frequency range starting from 10 kHz, up to 1 GHz. Type III bursts can be used for studying electron acceleration during solar flares, and magnetic field properties of the solar flares. In addition, a connection between hard X-ray (HXR) emission and type III bursts has been found but is not yet fully understood (Reid and Vilmer, 2017; Alissandrakis et al., 2015). Type III solar bursts can occur in various forms: isolated bursts that last from 1 s to 3 s, groups that last 10 minutes, and as a storm that lasts from 10 minutes to a few tens of hours (Mahender et al., 2020).

Type III solar radio bursts can be studied with various types of instruments. e-Callisto network instruments are widely used for studying type III bursts, e.g. Wijesekera et al. (2018), Mahender et al. (2020). Typically, e-Callisto devices are small, low-cost instruments. This also usually means lower sensitivity as well as lower time and frequency resolution. Low-Frequency Array (LOFAR)-class telescopes have been proven to excel in studying type III solar radio bursts (Morosan et al., 2014), and most recently by Zhang et al. (2020). LOFAR telescopes represent the current state-of-the-art technology.

In this work we will present some of the first type III solar radio bursts of the Solar Cycle 25, which were observed in May–June 2020. We will compare observational results between two different instruments which have rather different technical design and performance properties. Metsähovi Radio Observatory and Kilpisjärvi Atmospheric Imaging Receiver Array observations have been compared also earlier, but not when using the same frequency range (Kallunki, Uunila, and McKay-Bukowski, 2015). In addition, we present physical properties of the detected type III bursts and study their consistency between the instruments.

2. Instrumentation

Kilpisjärvi Atmospheric Imaging Receiver Array (KAIRA)¹ is located in Finnish Lapland and consists of a Low-Band Antenna (LBA) array approximately 34 m in diameter (center GPS: N 69:4.24 E 20:45.72), and a High-Band Antenna (HBA) array approximately 30 × 50 m (center GPS: N 69:4.26 E 20:45.66). Both arrays have 48 antennas. Each *LBA* is an inverted-V dipole with frequency range of 10–90 MHz. Each *HBA* is a tile containing 16 bow-tie antennas with frequency range of 110–270 MHz. All antennas are dual linear polarization. In this work, we will only use data from the LBA array.

The antenna and signal processing system chosen for KAIRA is the same as that used in the Low-Frequency Array (LOFAR) International Telescope, a radio telescope network intended for low-frequency astronomy, designed and produced by the Netherlands Institute for Radio Astronomy (ASTRON) and Dutch industry (van Haarlem et al., 2013). The main purpose of KAIRA is to demonstrate the capabilities of modern wide-band phased-array radio telescope technology for incoherent scatter radar measurements (Virtanen et al., 2014) and to operate as a passive ionospheric radio measurement facility (McKay-Bukowski et al., 2015).

Aalto University Metsähovi Radio Observatory² (MRO), located in southern Finland (GPS coordinates: N 60:13.04, E 24:23.35), installed a *crossed-dipole antenna* (CDA) manufactured by Reeve Observatory (Reeve, 2018) in October 2017. The new antenna, dubbed

¹Homepage: <https://www.sgo.fi/KAIRA/>.

²Homepage: <http://www.aalto.fi/metsahovi-radio-observatory>.

Table 1 Technical parameters of the METSOLA and KAIRA instruments.

Parameter	METSOLA	KAIRA
Frequency range (MHz)	18–90	10–90
Beam size	Omnidirectional, ≫ solar disc	0.03 λ rad
Integration time (s)	0.001	1
Sampling frequency	≤ 1 kHz	200 MHz
Temporal resolution (s)	0.25	1
Frequency resolution (kHz)	62.5	195.3

the Metsähovi Solar Observing Low-frequency Antenna METSOLA, has frequency coverage between 18 MHz and 90 MHz, and it expands *MRO*'s solar radio observing coverage (Kallunki et al., 2018a) to low frequencies. The antenna has two different polarization outputs (east–west and north–south), which makes it possible to study also the polarization properties of solar flares (Kallunki et al., 2018b). No significant differences in measurements between the linear polarizations were noted and, for this work, only the east–west polarization is shown for brevity. Key technical parameters of the two instruments are presented in Table 1.

The backend is a Callisto spectrometer (Callisto, 2018), designed to observe the dynamic spectra of solar flares and widely used for solar monitoring at frequencies below 1000 MHz. METSOLA operates in the frequency range of the classic solar radio burst types II, III and IV. At this frequency range it is possible to study properties of bursts in the solar corona.

3. Observations

Three type III solar radio bursts were observed with both instruments in May and June 2020. The overall activity behavior of the Sun was relatively low at that time. In May 2020, during the first two solar bursts, there were no classified active regions by the National Oceanic and Atmospheric Administration (NOAA) on the Sun. On June 5 there were two classified active regions (NOAA 12764 and 12765). The first and third events were classified as a sweep-frequency radio burst (RSP) by NOAA, and the second burst was classified as a GOES C9.3 event. The event came from the region 12765. The other two days (28 and 29 May) were without classified active regions; however, there was one rising and one fading unclassified active region on the Sun. All observed bursts were relatively weak. In Figures 1–3 the dynamic spectra of these radio bursts are shown. KAIRA spectra are raw data, the MRO data had average filtering conducted on them, where continuous transmissions and interferences have been filtered out. The first radio burst, on May 28, consists of two different drifting structures. They are marked in Figure 1 with red arrows. Both structures are analyzed separately (Tables 2–3). Other two events (Figures 2–3) show some harmonic emissions. For these cases, only the most powerful drifting structure is analyzed, hence other harmonics have a drifting profile similar to the fundamental drifting structure. The analyzed structures are marked with red arrows in Figures 1–3.

3.1. Radio Frequency Interference

One of the main problems when making radio astronomical observations at lower frequencies ($f \simeq 100$ MHz) is radio frequency interference (RFI). This frequency range is allocated for various services such as broadcasting, amateur and mobile. KAIRA instrument

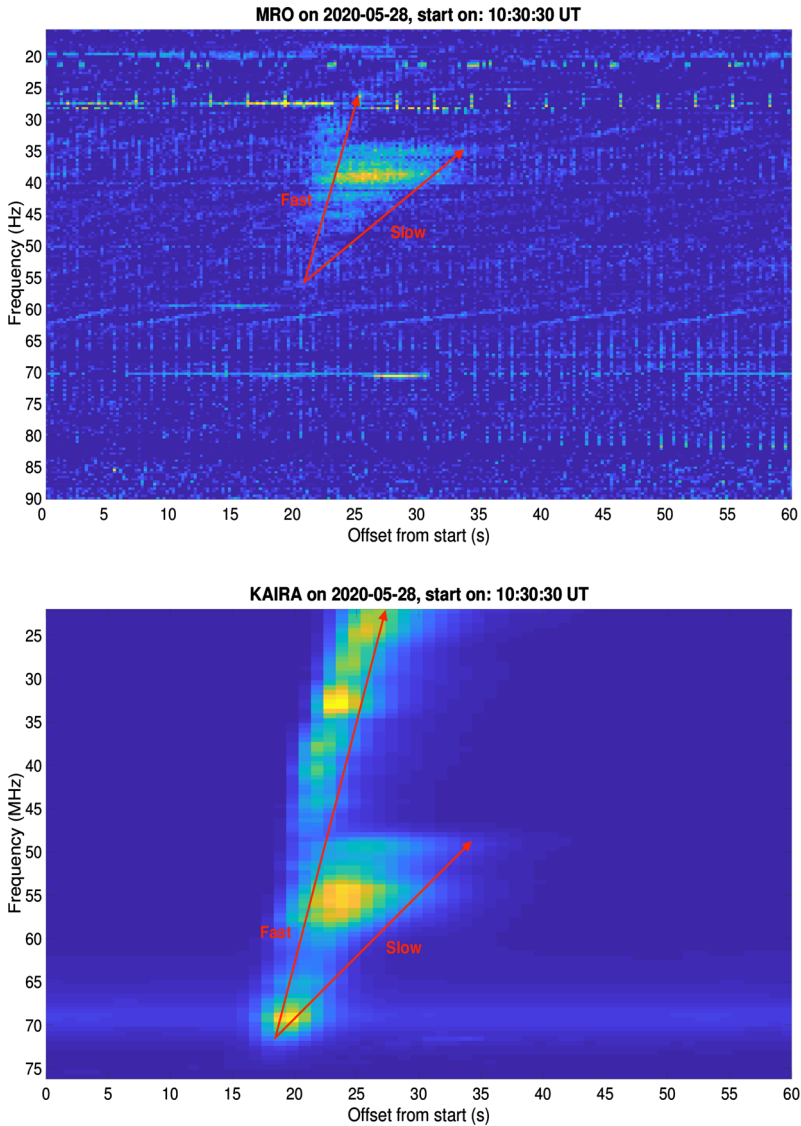


Figure 1 In the upper panel, the dynamic spectra recorded with the METSOLA long wavelength array antenna on 28 May 2020. In the lower panel, dynamic spectra recorded with the KAIRA on 28 May 2020. Radio burst consists of two different drifting structures or ribbons, which are marked in the plots. The properties of the “Fast” structure are shown in Table 2 and the “Slow” in Table 3.

is located at a very isolated place in Finnish Lapland, and thus the environment is ideal for low-frequency radio observations. In the KAIRA spectra we can see only some minor interference signals. METSOLA instrument, instead, is operated close to settlements, and in its dynamic spectra we can notice several interference signals. Some of the interference signals are self-generated by other electronic devices at the observatory but, for instance, radio location devices can also cause unwanted interference. It should be noted that there are no allocations to radio astronomy services within this band (20–90 MHz). The detected

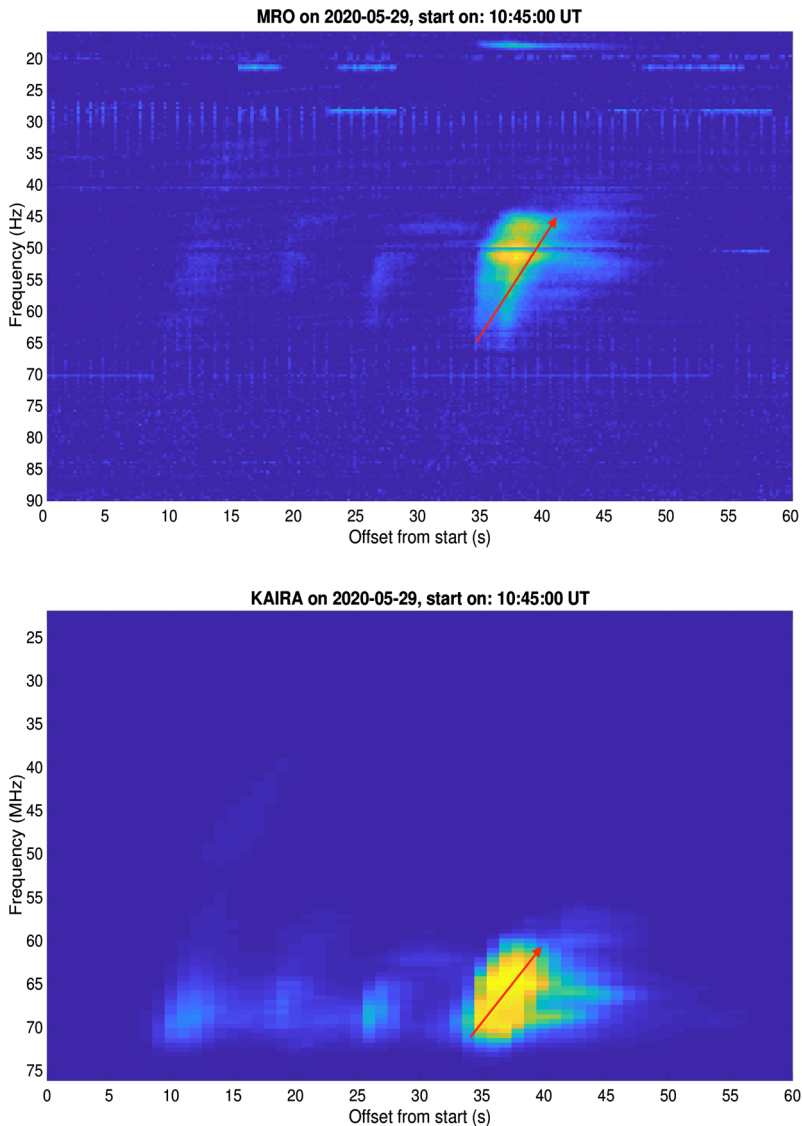


Figure 2 In the upper panel, dynamic spectra recorded with the METSOLA long wavelength array antenna on 29 May 2020. In the lower panel, dynamic spectra recorded with the KAIRA on 29 May 2020. The properties of the structure are shown in Table 4.

signals from powerful solar flares are strong enough to be observed even if the environment is not fully clear of RFI and other unwanted signals.

4. Results

The radio burst profiles and their dynamic spectra showed similar structures in both instruments. The frequency range of the METSOLA is a bit wider (15 MHz) than in KAIRA, thus

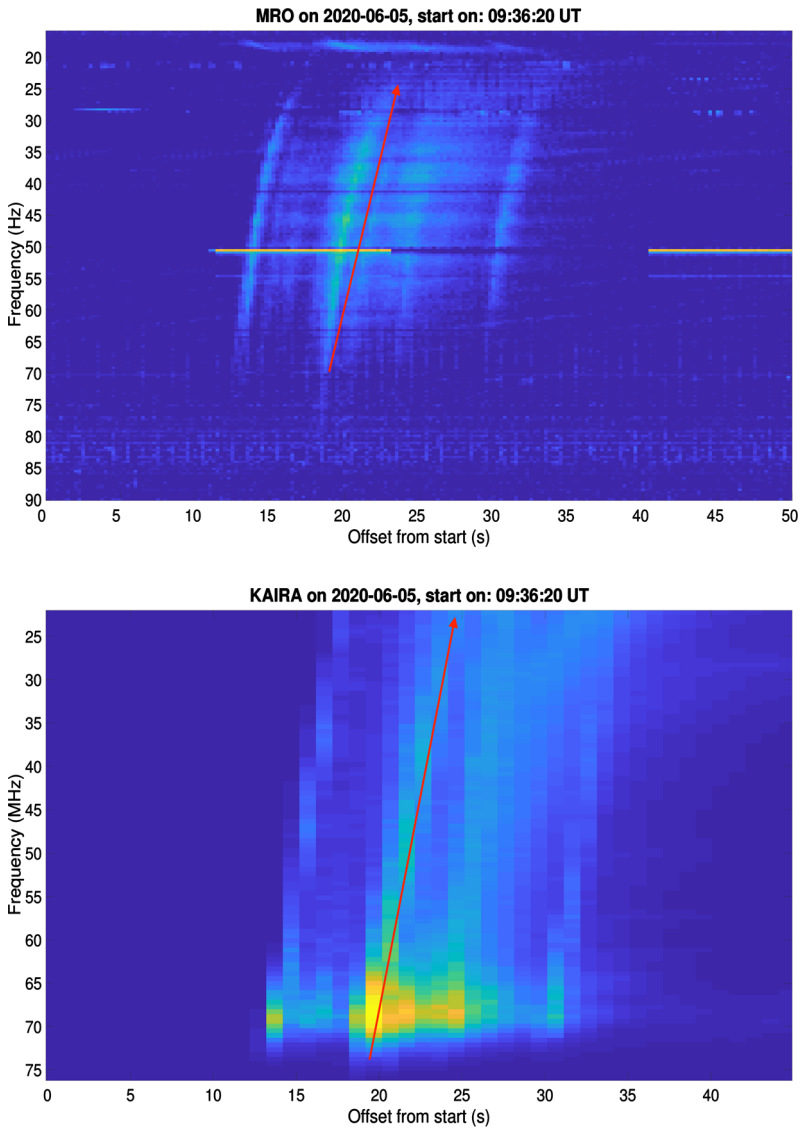


Figure 3 In the upper panel, dynamic spectra recorded with the METSOLA long wavelength array antenna on 5 June 2020. In the lower panel, dynamic spectra recorded with the KAIRA on 5 June 2020. The properties of the structure is shown in Table 5.

the results are not fully comparable. As mentioned already, KAIRA spectra are cleaner from RFI, which is seen as an almost clean background noise of the spectra.

Solar burst structures were detected between frequencies 22.3 MHz and 83.6 MHz. The detection times between the instruments were close to each other. Only 1–2 second difference was noticed. The accuracy of the simultaneity of the data is estimated to be within 1–2 second, e.g. due to the Callisto clock using inexpensive commercial off-the-shelf (COTS) components.

Table 2 Properties of the type III radio burst (fast) on 28 May 2020 starting at 10:30:50 UT.

Event – 28.5.2020 (Fast)	METSOLA	KAIRA
Drift rate (MHz/s)	11.7 ± 0.4	8.2 ± 0.6
Start distance (R_{\odot})	1.45 ± 0.03	1.4 ± 0.05
Stop distance (R_{\odot})	2.0 ± 0.03	1.99 ± 0.05
Speed (c)	0.23 ± 0.02	0.18 ± 0.03

4.1. Drift and Propagation Speeds, and Electron Densities of the Detected Solar Flare

It is possible to estimate the drift rate, the electron density, the speed, and even the height propagation properties of the solar type III radio burst on the basis of the observed dynamic spectra. The frequency drift rate of the type III solar radio burst can be estimated as (Pohjola- lainen et al., 2007)

$$\frac{df}{dt} = \frac{f_0 - f_1}{t_0 - t_1} \tag{1}$$

where f_0 and f_1 are the frequency of the burst at start (t_0) and end (t_1) of the observed burst, respectively. For example, in the 5 June 2020 event, the radio burst occurred 19 seconds (20 seconds in KAIRA) after the start and ended 24 seconds (26 seconds in KAIRA) after the start. Start and stop frequencies are 83.6 and 24.9 MHz (22.3 and 63.5 MHz in KAIRA). Thus, drifting rates are 11.7 and 6.9 MHz/s. The result is consistent with earlier observa- tion, e.g. Melnik et al. (2015), where observed drift rates varied between 0.44 MHz/s and 12 MHz/s for type III solar bursts.

The connection between the plasma frequency (ν_{pe}) and the electron density (n_e) can be estimated as (Bastian, Benz, and Gary, 1998; Pohjola- lainen et al., 2007)

$$\nu_{pe} \approx 9000 \times \sqrt{n_e}, \tag{2}$$

leading to electron densities (n_e) of $6.2 \times 10^6 \text{ cm}^{-3}$ and $8.7 \times 10^7 \text{ cm}^{-3}$, for 22.3 MHz and 83.6 MHz, respectively

After the electron densities (n_e) are defined for start and stop frequencies, corresponding distances (R) can be defined from the atmospheric density model. The propagation height can be estimated using the Newkirk 1st-order atmospheric density model (Wijesekera et al., 2018; Li, Cairns, and Robinson, 2009).

$$n_e = n_0 \times 10^{4.32 \frac{R_{\odot}}{R}} \tag{3}$$

where n_0 is $4.2 \times 10^4 \text{ cm}^{-3}$, R is distance from the solar center and R_{\odot} is the solar radius. This gives estimates for the propagation height of the solar flare at 22.3 MHz and 83.6 MHz as 1.3 R_{\odot} and 2.0 R_{\odot} , respectively, placing the observed event in the solar corona, as ex- pected. For the propagation speed approximation, we use the following equation (Wijesekera et al., 2018):

$$v = \frac{2 \frac{df}{dr} n_0}{f_{pe} \frac{dn}{dr}} \tag{4}$$

where $\frac{dn}{dr}$ is the change of electron density over distance. The propagation speed of the burst (5 June 2020) can be estimated 0.21c (0.28c at KAIRA) The other three events have been

Table 3 Properties of the type III radio burst (slow) on 28 May 2020 starting at 10:30:50 UT.

Event – 28.5.2020 (Slow)	METSOLA	KAIRA
Drift rate (MHz/s)	1.6 ± 0.4	2.5 ± 0.6
Start distance (R_{\odot})	1.45 ± 0.03	1.4 ± 0.05
Stop distance (R_{\odot})	1.69 ± 0.03	1.69 ± 0.05
Speed (c)	0.05 ± 0.02	0.06 ± 0.03

Table 4 Properties of the type III radio burst on 29 May 2020 starting at 10:45:34 UT.

Event – 29.5.2020 (Fast)	METSOLA	KAIRA
Drift rate (MHz/s)	4.2 ± 0.4	4.7 ± 0.6
Start distance (R_{\odot})	1.38 ± 0.03	1.4 ± 0.05
Stop distance (R_{\odot})	1.56 ± 0.03	1.61 ± 0.05
Speed (c)	0.16 ± 0.02	0.17 ± 0.03

Table 5 Properties of the type III radio burst on 5 June 2020 starting at 09:36:39 UT.

Event – 5.6.2020 (Fast)	METSOLA	KAIRA
Drift rate (MHz/s)	11.7 ± 0.4	6.9 ± 0.6
Start distance (R_{\odot})	1.3 ± 0.03	1.4 ± 0.05
Stop distance (R_{\odot})	1.91 ± 0.03	2.0 ± 0.05
Speed (c)	0.21 ± 0.02	0.28 ± 0.03

processed and analyzed in a similar way and the results are presented in Tables 2–5. The errors are estimated based on time and frequency resolutions of the dynamic spectra.

5. Conclusion

We have observed and reported the first type III solar radio bursts of Solar Cycle 25, simultaneously detected with two instruments that observed in different locations, and which have very different design and local environment but use approximately the same radio frequency range. We showed that the data quality and resolution of these instruments, both in time and frequency, are good enough for meaningful detailed burst analysis.

We have shown that both instruments are suitable for solar burst monitoring, and the results are comparable. It is interesting that also the very simple and low-cost instrument, METSOLA can provide burst profiles and dynamic spectra which are consistent with the state-of-the-art instrument, KAIRA. The results also emphasise the importance of the instrument site: close to settlements low-frequency observations inevitably suffer from a wide range of radio frequency interference. Thus, Finnish Lapland is an almost ideal location for such an instrument.

The northern location of KAIRA makes it possible to carry out extensive, uninterrupted solar observations during the summer months. This is a unique feature which should be utilized in future observing campaigns. Now that the Sun has entered a new activity cycle, both instruments will be able to gather data all the way from the relatively quiescent Sun toward the more active phases, and we expect to observe tens of new radio events with both instruments, including other solar radio burst types: I, II and IV.

KAIRA is a large facility and, as such, would normally be considered excessive for routine solar monitoring. However, it has much broader science objectives, ranging from atmospheric monitoring to astrophysics. It is expected to work alone, but also in conjunction with other radio telescopes and radars (McKay-Bukowski et al., 2015). KAIRA is a multipurpose instrument capable of conducting numerous experiments at once, thus requiring high technical performance and complexity. The solar monitoring component is just one of multiple observations that are running simultaneously on the instrument. The additional experimental capability provides an excellent opportunity to independently validate the measurements of METSOLA and other low-cost solar monitoring experiments.

In the future, additional RFI mitigation techniques will be considered for the data processing. For instance, real-time data processing algorithms could be a one solution. In addition, more attention should be given when selecting new electronic components in observatories. Some electronics, computing, reference clocks, etc. are enclosed in a high-integrity Faraday cage in both observatories. Nevertheless, the observatories are mindful of the need for local mitigation, and improvements will be made to such capabilities where possible.

MRO has also several other solar radio instruments for higher frequencies, up to 86 GHz. In future work we intend to combine data from all these instruments to study properties of solar bursts from lower chromosphere to upper corona in Solar Cycle 25.

Acknowledgements The low wavelength antenna presented here is manufactured by Reeve Engineering, <http://www.reeve.com>.

The Callisto spectrometer was designed by Christian Monstein, <http://www.e-callisto.org>.

KAIRA was funded by the University of Oulu and the FP7 European Regional Development Fund and is operated by Sodankylä Geophysical Observatory with assistance from the University of Tromsø. The work by Derek McKay is partly supported by the Academy of Finland project number 322535.

Funding Note Open access funding provided by Aalto University.

Conflict of interest The authors declare that there are no conflicts of interest.

Publisher's Note Springer Nature remains neutral with regard to jurisdictional claims in published maps and institutional affiliations.

Open Access This article is licensed under a Creative Commons Attribution 4.0 International License, which permits use, sharing, adaptation, distribution and reproduction in any medium or format, as long as you give appropriate credit to the original author(s) and the source, provide a link to the Creative Commons licence, and indicate if changes were made. The images or other third party material in this article are included in the article's Creative Commons licence, unless indicated otherwise in a credit line to the material. If material is not included in the article's Creative Commons licence and your intended use is not permitted by statutory regulation or exceeds the permitted use, you will need to obtain permission directly from the copyright holder. To view a copy of this licence, visit <http://creativecommons.org/licenses/by/4.0/>.

References

- Alissandrakis, C.E., Nindos, A., Patsourakos, S., Kontogeorgos, A., Tsitsipis, P.: 2015, *Astron. Astrophys.* **582**, A52. DOI.
- Bastian, T.S., Benz, A.O., Gary, D.E.: 1998, *Annu. Rev. Astron. Astrophys.* **36**, 131. DOI.
- e-Callisto: International Network of Solar Radio Spectrometers, a Space Weather. Instrument array. <http://www.e-callisto.org> (24.11.2018).
- Kallunki, J., Uunila, M., McKay-Bukowski, D.: 2015, *Astron. Nachr.* **336**, 566. DOI.
- Kallunki, J., Tornikoski, M., Tammi, J., Kinnunen, E., Korhonen, K., Kesäläinen, S., et al.: 2018a, *Astron. Nachr.* **339**, 204. DOI.
- Kallunki, J., Tornikoski, M., Oinaskallio, E., Kirves, P., Aatrokoski, J., Mujunen, A., et al.: 2018b, *Astron. Nachr.* **339**, 656. DOI.

- Li, B., Cairns, I.H., Robinson, P.A.: 2009, *J. Geophys. Res.* **114**, A02104. DOI.
- Mahender, A., Sasikumar Raja, K., Ramesh, R., Panditi, V., Monstein, C., Ganji, Y.: 2020, *Solar Phys.* **295**, 153. DOI.
- McKay-Bukowski, D., Vierinen, J., Virtanen, I.I., Fallows, R., Postila, M., Ulich, T., et al.: 2015, *IEEE Trans. Geosci. Remote Sens.* **53**, 1440. DOI.
- Melnik, V.N., Brazhenko, A.I., Konovalenko, A.A., Briand, C., Dorovskyy, V.V., Zarka, P., et al.: 2015, *Solar Phys.* **290**, 193. DOI.
- Morosan, D.E., Gallagher, P.T., Zucca, P., Fallows, R., Carley, E.P., Mann, G., et al.: 2014, *Astron. Astrophys.* **568**, A67. DOI.
- Pohjolainen, S., van Driel-Gesztelyi, L., Culhane, J.L., Manoharan, P.K., Elliott, H.A.: 2007, *Solar Phys.* **244**, 167. DOI.
- Reeve Observatory, Anchorage, Alaska USA. http://www.reeve.com/RadioScience/Antennas/ActiveCrossed-Dipole/LWA_Antenna.htm (26.11.2020).
- Reid, H.A.S., Vilmer, N.: 2017, *Astron. Astrophys.* **597**, A77. DOI.
- van Haarlem, M.P., Wise, M.W., Gunst, A.W., Heald, G., McKean, J.P., Hessels, J.W.T., et al.: 2013, *Astron. Astrophys.* **556**, A2. DOI.
- Virtanen, I.I., McKay-Bukowski, D., Vierinen, J., Aikio, A., Fallows, R., Roininen, L.: 2014, *J. Geophys. Res.* **119**, 10,528. DOI.
- Wijesekera, J.V., et al.: 2018, *J. Phys. Conf. Ser.* **1005**, 012046.
- Zhang, P., Zucca, P., Sridhar, S.S., Wang, C., Bisi, M.M., Dabrowski, B., et al.: 2020, *Astron. Astrophys.* **639**, A115. DOI.